Fluid Mechanics
2022; 8(1): 1-15
http://www.sciencepublishinggroup.com/j/fm
doi: 10.11648/j.fm.20220801.11
ISSN: 2575-1808 (Print); ISSN: 2575-1816 (Online)

Quinn's Law of Fluid Dynamics, Supplement #4 Taking the Mystery out of Permeability Measurements in Porous Media

Hubert Michael Quinn

Department of Research and Development, The Wrangler Group LLC, Brighton, USA

Email address:
hubert@wranglergroup.com

To cite this article:
Hubert Michael Quinn. Quinn's Law of Fluid Dynamics, Supplement #4 Taking the Mystery out of Permeability Measurements in Porous Media. *Fluid Mechanics.* Vol. 8, No. 1, 2022, pp. 1-15. doi: 10.11648/j.fm.20220801.11

Received: February 18, 2022; **Accepted**: March 15, 2022; **Published**: March 29, 2022

Abstract: The published literature on porous media is filled with erroneous and contradicting assertions relating to measurements of permeability. In this paper, we present a new and novel approach to remedy this situation, by demonstrating a standard methodology using a new fluid flow model. This model is different from any model currently in use and provides a unique analytical solution for the input variables underlying packed beds containing porous media of discrete particles, be they porous or nonporous in nature. The model is based upon the fundamental principles of the physics involved in fluid flow through packed beds which includes, amongst other things, a unique normalization coefficient which acts as an exchange rate between viscous and kinetic contributions, on the one hand, and certification, via a built-in methodology, on the other hand, that the Laws of Continuity are always adhered to. In addition, the model is thorough with respect to both wall effect and fluid path tortuosity, which means that a new Law of Fluid Flow in closed conduits is identified as a straight-line relationship between viscous normalized pressure drop, on one side of the equality sign, and normalized fluid flow, on the other side of the equality sign. The model is based upon the discovery of a new vector entity, n_p, the number of particles of a given diameter, say d_p, present in a packed conduit and, therefore, applies seamlessly to both packed and empty conduits which, in turn, enables its validation over 10 orders of magnitude of the modified Reynolds number. *This vector has never been identified heretofore* and is valid for all particle porosities which include fully porous particles, i.e., particles of free space and, hence, empty conduits are considered as packed conduits with particles of free space. The vector n_p specifies, simultaneously, the matched set of a given value for the *particle diameter* d_p and the *external porosity*, ε_0, in any packed conduit under study, much the same as a velocity vector specifies, simultaneously, the matched set of a given value for the *speed* and *direction* of a projectile or moving object. The model is explained herein and applied to a number of experimental studies, demonstrating a standardized methodology which guarantees an exact correlation between measured and calculated values in the permeability relationship, when reporting on actual experiments in closed conduits.

Keywords: Permeability, Pressure Drop, Viscous, Kinetic, Friction Factor

1. Introduction

In this paper we use the new fluid flow model, now known as The Quinn Fluid Flow Model (QFFM), to teach a new methodology to practitioners of fluid flow in closed conduits. This teaching applies seamlessly to both empty and packed conduits. The QFFM is to be found in the published literature [1] wherein it is written in its dimensionless form as:

$$P_Q = k_1 + k_2 C_Q \tag{1}$$

The term on the left-hand side of equation (1), P_Q, represents the pressure drop across the conduit normalized for both drag and viscous contributions. The right hand side of the equality sign represents the sum of the normalized viscous contributions, k_1, and the viscous normalized kinetic contributions, k_2C_Q. This equation is represented by a straight line on a xy plot of P_Q v C_Q, where the intercept on the y axis represents the value of k_1 and the slope of the line represents the value of k_2. This means that no matter what permeability result a practitioner may report, whether it pertains to an empty or packed conduit, it must by necessity fall on this straight line. This is an amazing discovery which is even more astonishing given the fact that it has been validated

over 11 orders of magnitude of the modified Reynolds number, i.e., over the entire fluid flow regime, from creeping flow to fully developed turbulence.

Why is this relationship so important and why has it not been identified heretofore? The answer to this question is that no one up until now was successful at developing a comprehensive equation which captures *all* the physics underlying fluid flow in closed conduits in a *single relationship*, including the wall effect elements of viscous boundary layer and roughened inner wall surface, on the one hand, and fluid path tortuosity and porosity, on the other hand. The current state of understanding in the art, unfortunately, treats the Reynolds number as the governing fluid flow parameter, which is a *fatal flaw* found in most every other fluid flow model. The QFFM not only contains all these missing elements but, in addition, has a built-in methodology which guarantees that the Laws of Continuity are adhered to every time the model is used to generate a solution to a permeability measurement. This is another critical feature of the QFFM not found in other extant fluid flow models, because they all embrace mathematical equations as though they were an integral part of the Laws of Nature, *which they are not.* Accordingly, applying mathematical equations, indiscriminately, which means without first grounding them by experiment, leads to erroneous results, something that is widespread in the published literature on this subject matter. We will now explain the underlying rationale for equation (1) and why it is a unique relationship dictated by the Laws of Nature.

Firstly, we explain in detail the basis for the universal constants, k_1 and k_2. Unlike the constants found in most other fluid flow models, i.e., the Ergun model [2], for instance, wherein their values are based upon a "residual" computation, i.e., the remainder after all other contributions are applied and are, therefore, fundamentally "fudge factors" used to create a correlation between measured and calculated values, these two parameters, found only in the QFFM, are based upon first principles of the Laws of Nature and, accordingly, are *not* fudge factors. In addition, the values of k_1 and k_2 are related to one another, to the extent that they are both derived from considerations driven by the manner in which Nature controls both viscous and kinetic contributions.

Viscous contributions are caused by the phenomenon of a fluid passing a solid obstacle in its flow path, wherein the interaction between the fluid and the solid object produces a retarding force which acts in the opposite direction to the fluid flow. In addition, the force generated is a function of the surface area of the interaction, i.e., the larger the surface area of contact the larger the retarding force. Thus, we can see that there is a *direct* proportionality between the retarding force and the surface area of the interaction. On the other hand, kinetic contributions are caused by the fluid flowing through a fixed orifice wherein the retarding force acting against the fluid is related to the size of the perimeter through which the fluid is forced to pass. Accordingly, our intuition tells us that the larger the perimeter, the smaller the retarding force, which means that there is an *indirect* proportionality between the retarding force and the perimeter of the opening in the orifice.

In considering an equation which captures both viscous and kinetic contributions, therefore, we begin with defining a control element of free space. To do this we, advantageously, take the case of a perfect sphere, since all the characteristics of a sphere are well-known in relation to its diameter D, i.e., surface area = πD^2, cross sectional area = $\pi D^2/4$, volume = $\pi D^3/6$. Next, we recognize that with respect to our control element of free space, the viscous contributions are *directly* related to the surface area of our sphere, i.e., πD^2, whereas the kinetic contributions are related to the *reciprocal* of the perimeter of the channel defined by our sphere, i.e., the cross-sectional area $\pi D^2/4$. In addition, since we need to add both viscous and kinetic contributions, we need to have an "exchange rate" between the two, much as we need an exchange rate between dollars and pounds sterling. Thus, we can see that the ratio between the surface area and the cross-sectional area of our sphere is the common denominator, representing this exchange rate, i.e., $[\pi D^2]/[\pi D^2/4] = 4$. Accordingly, to establish a controlling mechanism between viscous and kinetic contributions, we, advantageously, define our *unit sphere* as having a unit radius of $r_h = 4$, on the one hand, and our *unit channel* having a unit radius of $r_h = 1$ and thus a perimeter of $2\pi r_h = 2\pi$, on the other hand. We then establish the control volume of $(4/3)\pi r_h^3$ as the volume of our unit sphere. Next, we apportion this volume in accordance with our understanding of how the Laws of Nature controls viscous and kinetic contributions. This we accomplish by dividing the control volume of $(4/3)\pi r_h^3$ by $r_h = (4/3)\pi r_h^2 = 64\pi/3$, which represents our contact area direct proportionality normalization coefficient, i.e., k_1 and applying this same adjustment to our unit channel we get for the adjusted perimeter $2\pi r_h$, where $r_h = 4$, which when inverted to reflect an indirect (reciprocal) relationship = $1(8\pi)$, and represents our perimeter normalization coefficient, i.e., k_2. Finally, we also need to apply the same multiplier, i.e., $r_h = 4$ on the left-hand side of the equality sign in equation (1) to maintain the equality, i.e., $\Delta P/r_h$ which is embedded in P_Q. Thus, k_1 and k_2 are the *controlling elements* within the QFFM which maintains the balance between viscous and kinetic contributions in the dimensionless normalized equation (1).

Secondly, looking again to equation (1), we now examine the components of the viscous normalized kinetic term on the right hand side of the equality sign:

$$C_Q = \lambda Q_N = \lambda \delta R_{em} \tag{2}$$

Where $Q_N = \delta R_{em}$

This term represents one of the critical distinguishing features of the QFFM, as mentioned above, where we see that the well-known term, R_{em}, the modified Reynolds number, must be modified to accommodate two additional elements *not found in other fluid flow models*, i.e., the term:

$$\delta = \frac{1}{\varepsilon_0{}^3} \tag{3}$$

Where, δ represents a kinetic porosity normalization coefficient, where ε_0 = the external conduit porosity, and the term:

$$\lambda = (1 + W_N) \quad (4)$$

Where λ is a wall effect normalization coefficient, and W_N = the net wall-effect. We will not dwell here on a lengthy explanation of what the term ε_0 represents, since this external conduit porosity parameter is found in all other fluid models and is a well-understood parameter. Rather, we will drill down on the term W_N, the net wall effect, which is yet another distinguishing feature of the QFFM not present in other models.

The QFFM teaches that there are just five elements to the wall effect:

1. primary wall effect (W_1);
2. secondary wall effect (W_2);
3. residual secondary wall effect (W_{2R});
4. net wall effect (W_N) and finally,
5. wall normalization coefficient (λ).

The wall normalization coefficient $\lambda = 1 + W_N$, and enters the pressure flow relationship in the QFFM through the kinetic term. Accordingly, the λ parameter has no effect when the flow is laminar, i.e., when the kinetic contributions are negligible and the value of Q_N is very small, i.e., less than unity, say.

The net wall effect $W_N = W_1 + W_{2R}$, and will only manifest in measured pressure drop values where kinetic contributions are significant. In other words, the net wall effect has no impact on pressure drop in laminar flow.

The QFFM also defines five distinct categories of boundary conditions underlying the various fluidic milieus found in packed conduits. These categories are:

1A. Conduits packed with solid particles ($\varepsilon_p<1$) in which the ratio D/d_p is large, say greater than 10, and the particles have either smooth surfaces or are operated only in laminar flow. It will be appreciated that since the impact of the parameter λ is only manifest when kinetic contributions are significant, one cannot tell if particles are rough or smooth based upon permeability measurements taken only in laminar flow.

1B. This category is the same as 1A above except that the particle surfaces are manifestly rough. This category, then, represents permeability measurements taken at high values of Q_N, say $Q_N > 1$.

1C. This category is a special category in which the ratio D/d_p is close to 1 but the particles have a solid skeleton. This is an unusual case of a packed conduit, not typically found in practice, but created within the teachings of the QFFM, for a special experiment, wherein one can *independently* verify the external porosity value, ε_0, by counting the number of particles, n_p, having a given designated value of d_p-the spherical particle diameter equivalent of the particles- in any packed conduit under study. This experiment is critical to verifying the authenticity of the QFFM model, since it provides the independent means for reconciling the two partial fractions in conduits packed with nonporous particles, and the three partial fractions in conduits packed with partially porous particles, i.e., ε_0, ε_i and $(1 - \varepsilon_0)$.

2A. Conduits packed with fully porous particles ($\varepsilon_p=1$), i.e., an empty conduit or capillary, in which the ratio $D/d_p = 1$ and the inner wall surfaces of which are hydraulically smooth.

2B. This category is the same as 2A above except that the inner wall surfaces are rough and permeability measurements are taken at sufficiently high values of Q_N where the wall roughness punches through the viscous boundary layer.

2. Theory

No wall Effect

A packed conduit with solid particles and a ratio of D/d_p which is large, say greater than 10, will have no wall effect when the permeability measurements are taken in laminar flow. As shown in Figure 1, all our samples are packed conduits with smooth solid particles. They have no wall effect which means they all fall on the line for $\lambda = 1$ which is apparent on the plot of Θ versus Q_N. The source for these samples can all be found in the designated references herein [3-6].

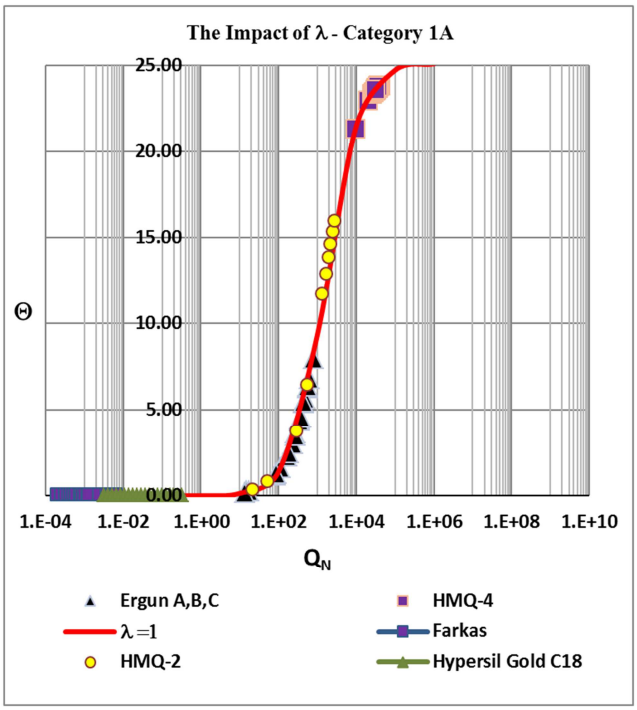

Figure 1. *No wall Effect.*

2.1. The Primary Wall Effect (W_1)

The primary wall effect has the symbol W_1 and is a derivative of two distinct parameters defined in the QFFM.

Firstly, W_1 is a derivative of the dimensionless viscous boundary layer $\beta_0 = (k_1/k_1 + k_2 Q_N)$, where $k_1 = (64\pi/3)$ and $k_2 = (1/8\pi)$, and are the universal Quinn constants. $Q_N = \delta R_{em}$ is the fluid current (Quinn number). The symbol R_{em} stands for the well-known modified Reynolds number and $\delta = (1/\varepsilon_0^3)$.

Secondly, the formula for the primary wall effect is $W_1 = (\beta_0^{(1/3)}/\tau)$. It is, therefore, also a derivative of the tortuosity factor, $\tau = \delta\gamma$, where $\gamma = (n_{pq}D/L)$ is a structural feature of the flow embodiment under study (packed or empty conduit), where n_{pq} is the volume of the empty conduit expressed in terms of number of particle equivalents having a diameter of d_p.

2.1.1. W_1 Has Its Maximum Value $W_1 = 5.33$ Approx

There is just one operating condition when the value of the primary wall effect has its maximum value of 5.33 approx. This condition exists when D/d_p has its minimum value of unity [$(D/d_p) = 1.0$], which only occurs in a conduit packed with particles of free space wherein the particles are fully porous ($\varepsilon_p = 1$), i.e., an empty conduit, and the value of Q_N is very small. In this scenario, the tortuosity coefficient, τ, is *relatively small* but always has a constant value, which results in a thick boundary layer when the value of Q_N is very small (Laminar flow). As the value of Q_N increases, however, the boundary layer starts to dissipate which reduces its thickness and eventually approaches a value of zero at very large values of Q_N (fully developed turbulence).

2.1.2. W_1 Manifestation

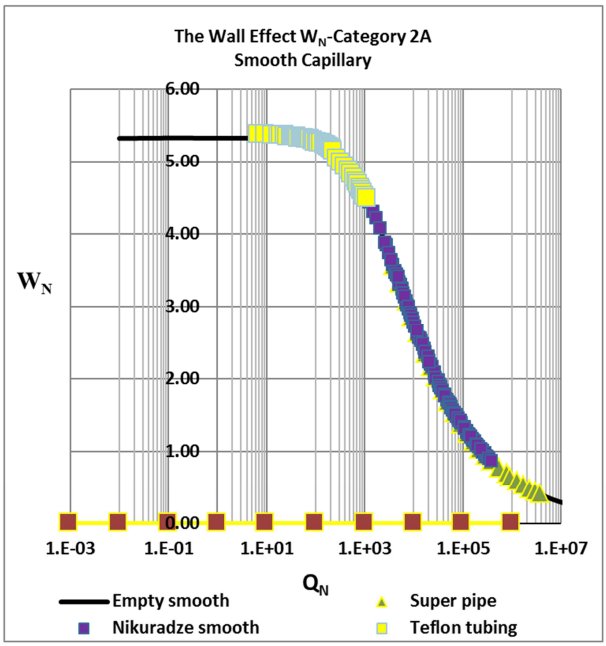

Figure 2. *The Primary Wall Effect maximum value.*

The primary wall effect W_1 will only manifest when the value of (D/d_p) is very small, such as in an empty conduit, and when kinetic contributions are significant. At very high values of Q_N, on the other hand, where the boundary layer is totally depleted, the value of $W_1 = 0$, and thus will not manifest at all. Additionally, when D/d_p is very large, say greater than 10, which only occurs in a conduit packed with solid particles, the tortuosity coefficient, τ, is very large and this reduces the thickness of the boundary layer to an insignificantly small value, hence the value for $W_1 = 0$ approx., at all values of Q_N. As shown in Figure 2 for category 2A, an empty conduit with hydraulically smooth walls, the net wall effect will have a maximum value of $W_1 = W_N = 5.33$ approx., at low values of the Quinn number. This represents the steady/stable viscous boundary layer adjacent to the channel wall. At a value of $Q_N > 1$ (approx.), the viscous boundary layer starts to be dissipated and the value of W_1 will decrease until it reaches a value of zero at very high values of the Q_N number, i.e., fully developed turbulence. This is shown in Figure 3 by the third party published works of Nikuradze [7] and the Princeton Super Pipe smooth wall data [8, 9], which falls in this decreasing region of the viscous boundary layer because all the measurements were taken at relatively high values of Q_N, i.e., $Q_N > 1$. Included on this plot also is the data measured by the current author in a smooth walled Teflon tubing at lower values of Q_N, to establish the viscous boundary layer baseline.

It will be appreciated that $W_1 = W_N$, the net wall effect, for all values of Q_N in a smooth walled empty conduit.

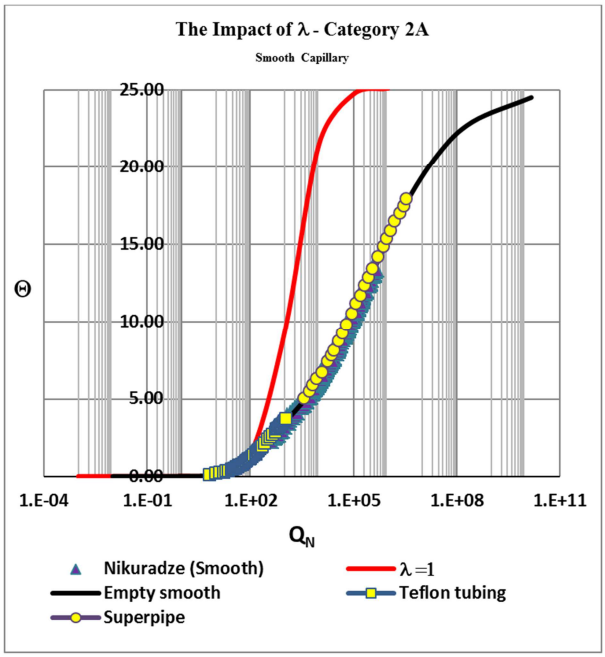

Figure 3. *The Primary Wall Effect selected studies.*

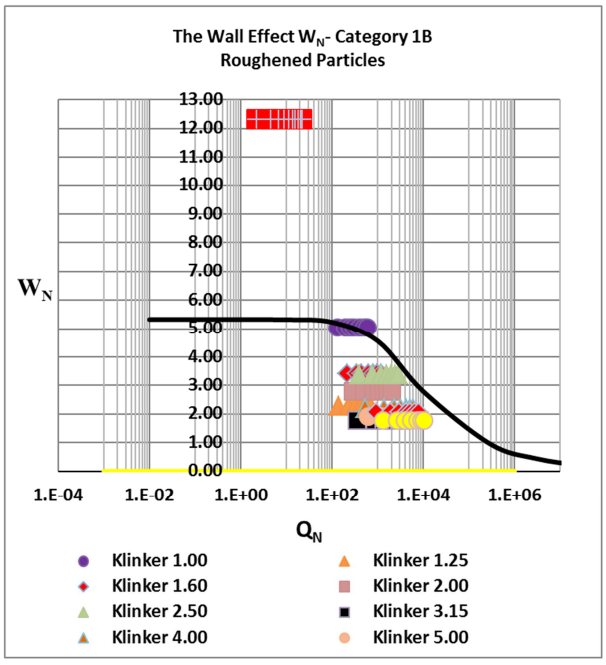

Figure 4. *The secondary wall effect.*

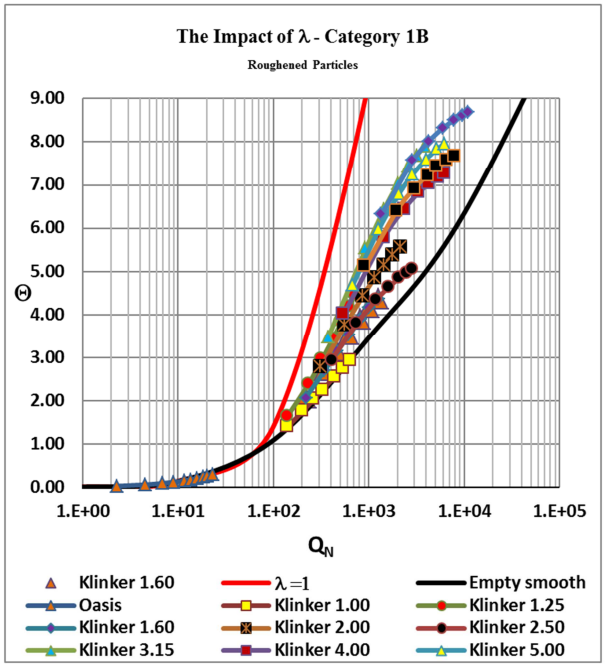

Figure 5. *The secondary wall effect comparison.*

2.2. The Secondary Wall Effect (W_2)

The secondary wall effect has the symbol W_2 and is a derivative of the sand-grain roughness, k, and the diameter of the hypothetical fluid channel d_c. In fact, it is proportional to the ratio of the two where $W_2 = 30\ k_{dc}^{(1/3)}$ and $k_{dc} = k/d_c$ where k is the sand grain roughness and $d_c = d_p/[abs(1-\varepsilon_0)]$ is the diameter of the hypothetical fluid channel. The constant of proportionality is the value of 30, which is due to end effects. It will be appreciated that d_p stands for the spherical particle diameter equivalent of the particles in the conduit, either packed with solid particles ($\varepsilon_p < 1$) or particles of free space ($\varepsilon_p = 1$), i.e., an empty conduit, where ε_p stands for the *particle* porosity.

2.2.1. The Value of W_2 Is Not Always Constant

When the particle sand grain roughness value, k, has a value greater than zero, i.e., $k > 0$, the value of W_2 will be a function of the channel diameter d_c. A constant value of k, therefore, will not always produce the same value of W_2. The larger the value of the channel diameter d_c, the smaller is the value of W_2 for any given value of the sand grain roughness coefficient k. In other words, wall roughness has less of an impact at larger diameters of the channel.

2.2.2. The Value of W_2 Is Only Apparent at High Values of Q_N When (D/d_p) Is Very Small

Because, in an empty conduit, the viscous boundary layer may sometimes be greater in depth than the sand grain roughness value, k, in which case it will mask the effect of the wall roughness, W_2 will only manifest at high values of Q_N when the boundary layer has been reduced and the sand grain roughness punches through the viscous boundary layer.

2.2.3. The Value of W_2 Is Always Apparent When (D/d_p) Is Very Large and Q_N Is Very Large

In packed conduits where the value of (D/d_p) is very large, i.e., a typical packed conduit with solid particles, the secondary wall effect, W_2, manifests at all high values of Q_N wherein the kinetic contributions are significant. As shown in Figures 4 and 5, all 10 Klinker packed conduits in our study here with solid particles, from the Buchwald et al article, have a range of value for $W_2 = W_N$ between 1.0 and 6.0 approx. [10]. As compared to smooth walled data, all the Klinker data fall under the boundary layer line for smooth walls. This is because, due to the very high tortuosity of the fluid flow in the Klinker conduits, there is no boundary layer and hence $W_1 = 0$, i.e., the primary wall effect is negligible. This plot also includes a sample measured by this author (HMQ-1) which has a net wall roughness of 12.0, i.e., $W_N = 12$ [1].

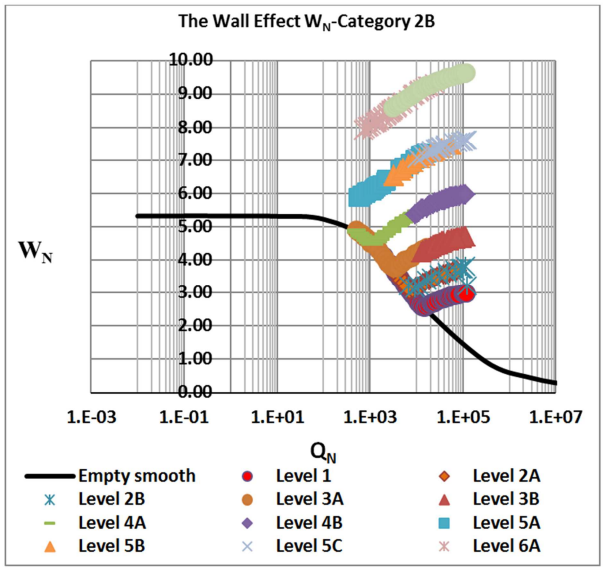

Figure 6. *The Residual Secondary Wall Effect.*

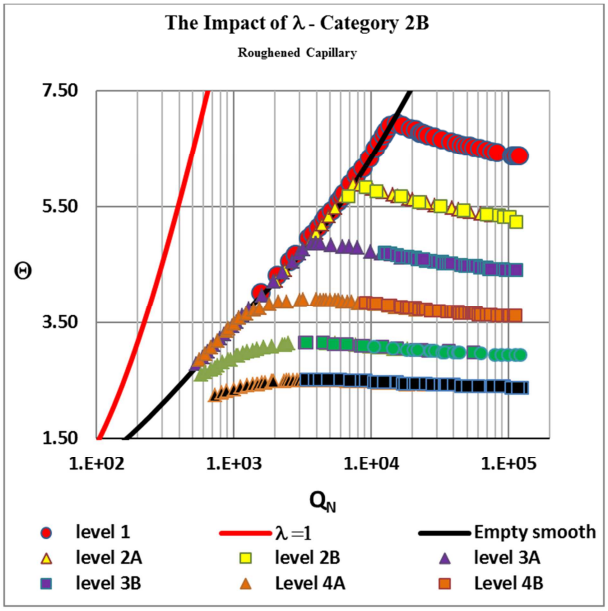

Figure 7. *Residual Secondary Wall Effect.*

2.3. The Residual Secondary Wall Effect (W_{2R})

The residual secondary wall effect is a derivative of both the primary and secondary wall effects. Indeed, it is a derivative of the difference between the two, i.e., $W_{2R} = W_2 - W_1^{(1.2)}$.

2.4. The Net Wall Effect (W_N)

The net wall effect is the sum of the primary wall effect and the residual secondary wall effect, i.e., $W_N = W_1 + W_{2R}$. It is the net wall effect W_N that influences the measured pressure drop. In our plot in Figure 6 the samples have both a primary and secondary wall effect and represent the six levels of sand-roughened empty conduits from Nikuradze [11] (levels 1-6 in legend). Note that all 6 of the Nikuradze roughened conduits fall on the opposite side of the boundary layer line, represented by the smooth-walled data than does the Klinker data shown above in Figure 4. This is because, although some of the Nikuradze measurements were taken in the region where the boundary layer masked the secondary wall effect, i.e., the sand grain roughness was buried in the boundary layer, most of the Nikuradze measurements were taken at high enough values of Q_N, where the sand grain roughness punched through the boundary layer, hence the appearance of the line to the right of the boundary layer line. This shows how the residual secondary wall effect, W_{2R}, manifests in the overall value of λ.

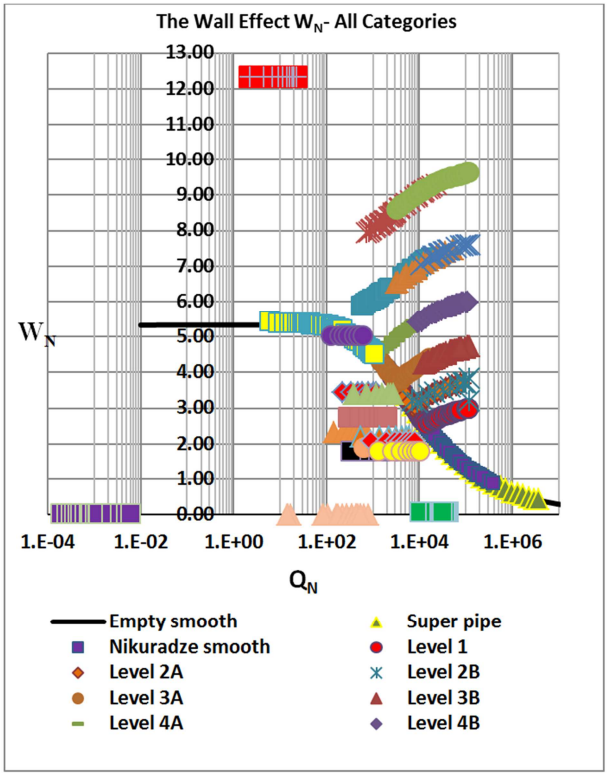

Figure 8. *The Impact of ⌊.*

2.5. The Wall Normalization Coefficient (λ)

We define the wall normalization coefficient $\lambda = (1 + W_N)$. This is the parameter that accounts for the impact of wall effect in fluid dynamics. When there is no wall effect, i.e., $W_N = 0$, the value of $\lambda = 1.0$.

As can be seen from Figure 7, in the QFFM, a plot of Θ versus Q_N normalizes for all samples, and allows us to view their fluid dynamic profile in one single frame of reference. All the Klinker packed conduits fall between the line for λ = 1 (no wall effect) and the line for empty conduits with smooth walls which represents the viscous boundary layer. This is because the Klinker samples have no primary wall effect and their sand grain roughness equivalent corresponds to a range of values of λ less than 6.0 approx. All the six levels of the roughened Nikuradze conduits, on the other hand, falls on the right hand side of the boundary layer line. This is because the roughened samples have a residual secondary wall effect W_{2R} due to the protrusion of the sand-grain roughness through the viscous boundary layer.

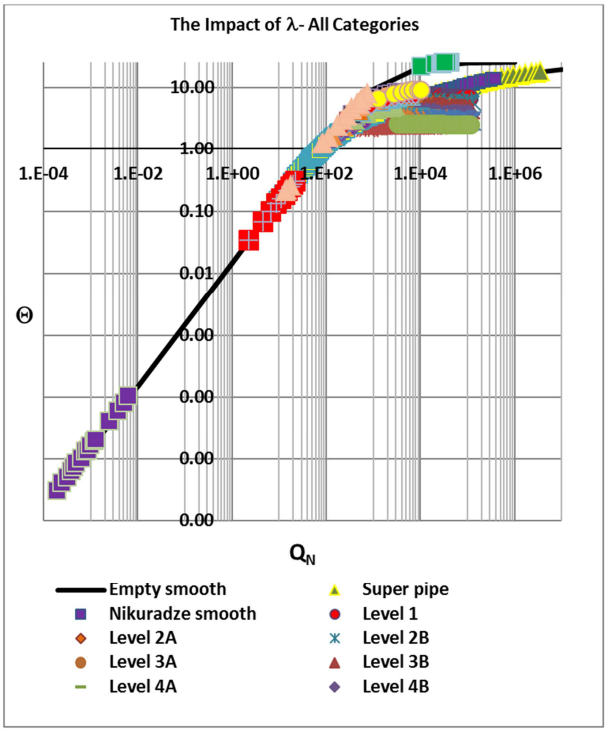

Figure 9. *The Impact of ⌊.*

As shown in Figure 9, the QFFM has been validated over 11 orders of magnitude of the modified Reynolds number, from the low values of the Farkas packed conduit, to the high values of the Nikuradze and Princeton studies pertaining to empty conduits. This is only possible with the QFFM because it is the only fluid flow model extant that seamlessly embraces both types of fluid flow embodiments. It will be appreciated that this reality, in turn, is dictated by the Laws of Nature, since pressure drop is the price one pays for studying the extreme fringes of the fluid flow regime. Thus, packed conduits with solid particles cannot be studied at very *high* values of the modified Reynolds number because the pressure drops would be prohibitively high, on the one hand, and, on the other hand, empty conduits cannot be studied at

very *low* values of the modified Reynolds number because the pressure drops would be prohibitively low.

3. Restoring the Dimensional Manifestation of the QFFM

Now that we have identified all the elements of the normalized relationship in equation (1) and how they relate to one another, let us now restore the dimensional manifestation of the QFFM.

Let $P_Q = \Delta P/(r_h n_v)$ and $R_{em} = n_k/n_v$ and substituting into equation (1) gives:

$$\frac{\Delta P}{r_h n_v} = k_1 + k_2 \delta\lambda \frac{n_k}{n_v} \quad (5)$$

where, n_v and n_k are the actual viscous and kinetic contributions, respectively. Thus, equation (5) is the explicit form of equation (1) based upon our control volume for our unit sphere.

Multiplying equation (5) across by $(r_h n_v)$ and substituting for k_1 and k_2 gives:

$$\Delta P = \frac{256\pi n_v}{3} + \frac{\delta\lambda n_k}{2\pi} \quad (6)$$

Let $n_v = \mu_s \delta\eta L/d_c^2$ and $n_k = \mu_s^2 \delta\rho_f L/d_c$ and substituting into equation (6) gives:

$$\Delta P = \frac{256\pi\mu_s\delta\eta L}{3{d_c}^2} + \frac{\delta\lambda{\mu_s}^2\delta\rho_f L}{2\pi d_c} \quad (7)$$

Where $\mu_s = 4q/(\pi D^2)$ is the fluid flux (superficial fluid velocity), q = the fluid volumetric flow rate, η = the fluid absolute viscosity and ρ_f = the fluid density.

Dividing equation (7) across by L gives the pressure gradient as:

$$\frac{\Delta P}{L} = \frac{256\pi\mu_s\delta\eta}{3{d_c}^2} + \frac{\delta^2\lambda{\mu_s}^2\rho_f}{2\pi d_c} \quad (8)$$

Equation (8) represents the *general* dimensional permeability equation within the QFFM based upon the flow term expressed as the superficial velocity. We point out here, for the purpose of making the QFFM more transparent and more easily understood, that when equation (8) is arranged in the format of the Ergun fluid flow model, by the grouping of certain terms in the QFFM, we can identify the Q-modified Ergun model coefficients of A and B as follows:

$$A = 256\pi/3 = 268.19 \text{ approx., and } B = \delta\lambda/2\pi \quad (9)$$

Accordingly, in *direct contradiction* to the Ergun model's expressed values of 150 and 1.75 for the viscous and kinetic constants, respectively, the Q-modified Ergun model's value, dictated by the QFFM, for the viscous constant is always A = 268.19 approx., a constant value, and the kinetic coefficient is $B = \delta\lambda/2\pi$, the latter, a variable, and *not* a constant.

We now identify a *special* case which applies to an empty conduit by applying the two limiting boundary conditions of, (1) $d_p = D$ and, (2) $n_p = -n_{pq}$ and substituting into equation (8) gives:

$$\frac{\Delta P}{L} = \frac{256\pi\mu_s\eta}{24D^2} + \frac{\lambda{\mu_s}^2\rho_f}{128\pi D} \quad (10)$$

Where n_p = the number of particles of diameter d_p present in the packed conduit.

Equation (10) represents the permeability equation within the QFFM which applies to an empty conduit based upon the flow term expressed as the superficial velocity.

We wish to point out here that, in the QFFM, the absolute value of the particle fraction in a packed conduit is defined as:

$$\text{abs}(1-\varepsilon_0) = \frac{n_p}{n_{pq}} \quad (11)$$

This is a critical differentiating element of the QFFM not found in any other fluid flow model, because it certifies that the particle fraction, $(1-\varepsilon_0)$, and the external porosity, ε_0, of a packed conduit are *dependent* variables, not *independent* variables, as is typically found in most, if not all, other fluid flow models. The parameter n_p is the independent packed conduit variable based upon the other independent packed conduit variables of D, L, which specifies, simultaneously, the values of d_p and ε_0. *We suggest that the reader study the original QFFM publication paying special attention to the discussion therein of the parameter, n_p, a vector quantity driving the external porosity values in both empty and packed conduits.* Without prior knowledge of the value of n_p, therefore, the QFFM *will not allow* a practitioner to execute the permeability equation, and this is the built-in mechanism that guarantees that the Laws of Continuity are always adhered to when the QFFM is used to create a solution in any experiment under study. Consequently, in order to identify the value of n_p, one must be able to determine accurately the volume occupied by a single particle of diameter d_p. *This is the methodology embedded in the QFFM that prevents the flawed practice, commonly found in other fluid flow models, of using nominal and independently derived values for d_p and ε_0, when using fluid flow models to calculate important variables.*

4. Methods

We will now describe the standardized approach we recommend for any empirical study involving permeability measurements in closed conduits.

10-Step Standard method protocol:

Step 1. Make a plot of the measured pressure drop versus the measured flow rate data.

Step 2. Determine the Forchheimer "fudge factor" coefficients a, and, b. [12]

Step 3. Refine the Forchheimer values of a, and, b from above, to best correlate the measured data.

Step 4. Apply the QFFM simultaneous solution to back-calculate and identify the values of, d_c and ε_0, assuming that the value of $W_N = 0$, i.e., $\lambda = 1$ (no wall effect).

Step 5. Correlate the measured and calculated values for

ΔP using the QFFM by setting the value of λ.

Step 6. Determine the Q-Modified Ergun model coefficients, A, and B.

Step 7. Determine the Universal Constants, k_1 and k_2.

Step 8. Compare the measured and calculated pressure drops.

Step 9. Document a first summary table.

Step 10. Document a second summary table.

Worked Example 1-The Buchwald et al Article

The data contained in this example represents a packed conduit with nonporous particles, $\varepsilon_p = 0$, which corresponds to our category 1B mentioned above. It is important to point out that the authors of the Buchwald et al paper [10] determined the external porosity values by measuring the mass of particles packed into each conduit and using the known bulk density of the solids to establish the value of ε_0. Since this process establishes the particle fraction in the packed conduit, $(1-\varepsilon_0)$, by default, i.e., it is a dependent variable, and provides no information relating to particle shape or size, the QFFM uses the independent methodology of establishing n_p, the number of particles present with a value of d_p for particle diameter-the spherical particle diameter equivalent- to reconcile the partial fractions within the packed conduit. This is accomplished by using the formula for a sphere to determine the volume occupied by a single particle of diameter d_p.

Using this worked example we will demonstrate our proposed methodology by evaluating the results of the Klinker particle permeability measurements which were the subject of the Buchwald et al paper. We will demonstrate our methodology by focusing on just one (sample # 1.00) out of ten of the packed conduits in that study.

Step 1. Make a plot of the measured pressure drop versus the measured flow rate data.

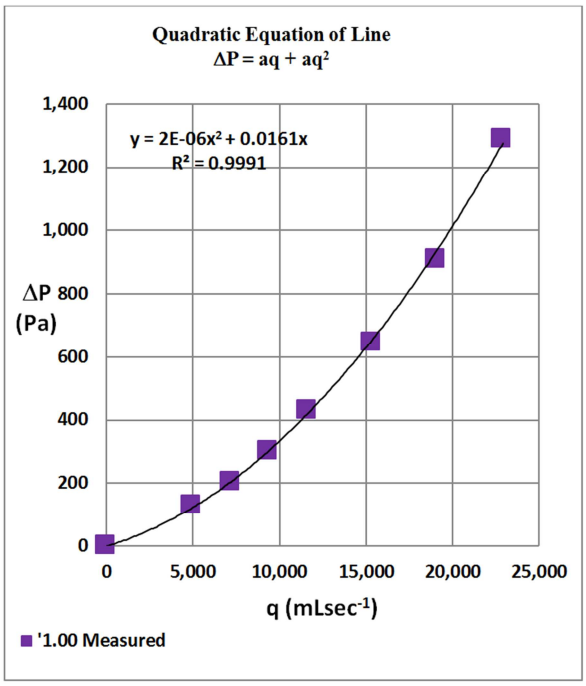

Figure 10. *Pressure versus flow rate.*

In Figure 10 we show a plot of the measured pressure drops in units of Pascal versus measured flow rate in units of mL/sec for sample 1.00 of the Klinker study. The measured data may now be reported as the 2nd order polynomial equation of the line, shown in the plot. This allows any practitioner to reproduce the measured results easily.

Step 2. Determine the Forchheimer "fudge factor" coefficients a and b.

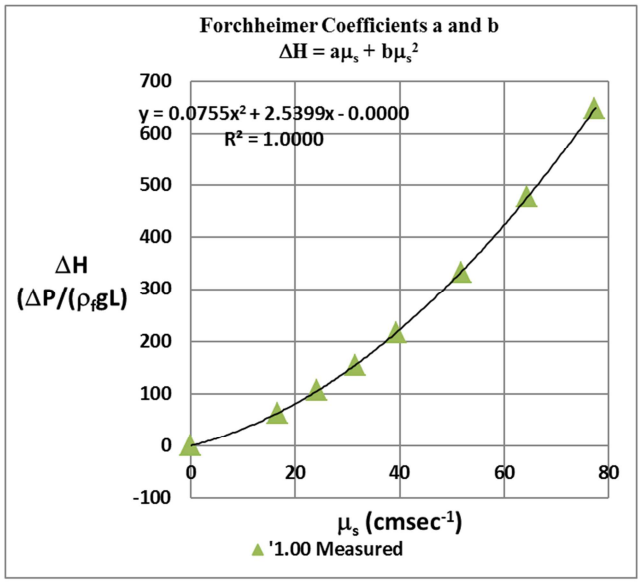

Figure 11. *Hydraulic conductivity versus fluid velocity.*

As shown in Figure 11, the second order polynomial fit to the measured data identifies the Forchheimer coefficients a, and, b. Once again, this equation of the line makes it easy for any practitioner to reproduce the data.

Step 3. Refine the Forchheimer values of a, and b, from above to best correlate the measured data.

This step is accomplished by comparing the calculated values for $\Delta H_{(meas)} = \Delta P_{(meas)}/(\rho_f g L)$, the hydraulic gradient based upon measured values, and $\Delta H_{(For)} = a\mu_s + b\mu_s^2$, the hydraulic gradient based upon the Forshheimer fudge factor coefficients. To do this, we recommend adjusting the value of a, until both values of ΔH are identical, at the lowest flow rate measurement, and adjusting the value of b, until both values of ΔH are identical at the highest flow rate. This step is necessary because viscous and kinetic contributions are based upon completely different fluid flow characteristics. Accordingly, an "average" algorithm does not produce the best fit to the measured permeability data.

Step 4. Apply the QFFM simultaneous solution to back-calculate the values of d_c and ε_0 when $\lambda = 1$.

Using the optimized Forchheimer values for a, and, b, in step 3 above, we can now apply the QFFM simultaneous solution, which is contained in equations 18 and 19, described in reference [13]. We recommend that the practitioner set up a spreadsheet to carry out this back-calculation, as shown below.

Initially, as shown in Table 1 below, set the independent

parameter λ=1 and apply the optimized Forchheimer coefficients, a, and, b, for all 7 flow rates measured. Note that in this initial back-calculate attempt, *for this worked example*, the QFFM does not return the correct pressure drop, i.e., $\Delta P_{(calc)}$ does not match the $\Delta P_{(meas)}$. This means that the particles in this worked example are not smooth because if they were smooth, the pressure drops would correlate at a value λ = 1 and, thus, a value of k = 0. Therefore, this initial trial tells us that these particles are not hydraulically smooth.

Table 1. *First back-calculation.*

Sample	q	$\Delta P_{(meas)}$	μ_s	a	b	$\Delta H_{(FOR)}$	$\Delta H_{(meas)}$	λ	d_c	ε_0	$\Delta P_{(calc)}$
ID	**mL/sec**	**Pa**	**cmsec^{-1}**	**s/cm**	**s^2/cm^2**	**none**	**none**	**none**	**cm**	**none**	**Pa**
Klinker	**0**	**0**	**0.00**			**0.00**	**0.00**				**0**
	4,956	127	16.76	2.5511	0.0754	63.93	63.93	1.00	0.475	0.407	300
	7,147	206	24.17	2.5511	0.0754	105.69	103.27	1.00	0.475	0.407	569
1.00	9,339	304	31.58	2.5511	0.0754	155.73	152.45	1.00	0.475	0.407	922
	11,604	431	39.24	2.5511	0.0754	216.16	216.38	1.00	0.475	0.407	1,376
	15,294	646	51.72	2.5511	0.0754	333.56	324.56	1.00	0.475	0.407	2,306
	19,073	911	64.50	2.5511	0.0754	478.11	457.34	1.00	0.475	0.407	3,506
	22,891	1,293	77.41	2.5511	0.0754	649.13	649.13	1.00	0.475	0.407	4,971

Step 5. Correlate the values of $\Delta P_{(meas)}$ and $\Delta P_{(calc)}$ by solving for the value of λ.

Table 2. *Second back-calculation.*

Sample	q	$\Delta P_{(meas)}$	μ_s	a	b	$\Delta H_{(FOR)}$	$\Delta H_{(meas)}$	λ	d_c	ε_0	$\Delta P_{(calc)}$	k
ID	**mL/sec**	**Pa**	**cmsec^{-1}**	**s/cm**	**s^2/cm^2**	**none**	**none**	**none**	**cm**	**none**	**Pa**	**cm**
Klinker	**0**	**0**	**0.00**			**0.00**	**0.00**				**0**	**0.0**
	4,956	127	16.76	2.5511	0.0754	63.93	63.93	5.99	0.261	0.605	127	0.00120
	7,147	206	24.17	2.5511	0.0754	105.69	103.27	5.99	0.261	0.605	211	0.00120
1.00	9,339	304	31.58	2.5511	0.0754	155.73	152.45	5.99	0.261	0.605	310	0.00120
	11,604	431	39.24	2.5511	0.0754	216.16	216.38	5.99	0.261	0.605	431	0.00120
	15,294	646	51.72	2.5511	0.0754	333.56	324.56	5.99	0.261	0.605	664	0.00120
	19,073	911	64.50	2.5511	0.0754	478.11	457.34	5.99	0.261	0.605	952	0.00120
	22,891	1,293	77.41	2.5511	0.0754	649.13	649.13	5.99	0.261	0.605	1,293	0.00120

Note that, as shown in Table 2, in this second and final back-calculate attempt, the QFFM identifies the value of 0.261 cm for d_c, and the value of 0.605 for ε_0, corresponding to the set value of 5.99 for λ. Note also that the values for $\Delta P_{(calc)}$ and $\Delta P_{(meas)}$ are a virtual perfect match at all flow rates measured, allowing for experimental error. Finally, note that the value of λ which correlates the data is 5.99 and corresponds to a value of k = 0.00120 cm i.e., 12 μm approx. Thus, this result tells us that this packed conduit can be represented as a hypothetical flow channel with diameter d_c = 0.261 cm and a wall sand grain roughness of 12 μm approximately, i.e., it establishes the roughness of the particles on the same relative basis as the classical sand grain roughness taught by Nikuradze.

Step 6. Determine the Q-Modified Ergun model coefficients, A, and B.

As shown in Figure 12, we can now establish the Q-modified Ergun coefficients, A, and, b, because we now have defined the modified Reynolds number in step 5 above. Note that the values on both axes are all derived based upon measured values. The best straight line is always achieved with an intercept value set of 268.19.

As shown in Figure 13, the values of k_1 and k_2 are identified. Additionally, note that the relevant governing parameter on the x- axis is $C_Q = \delta\lambda R_{em}$, not the Reynolds number R_{em}. Again, the best straight-line fit is achieved when the intercept of the line = 67.05.

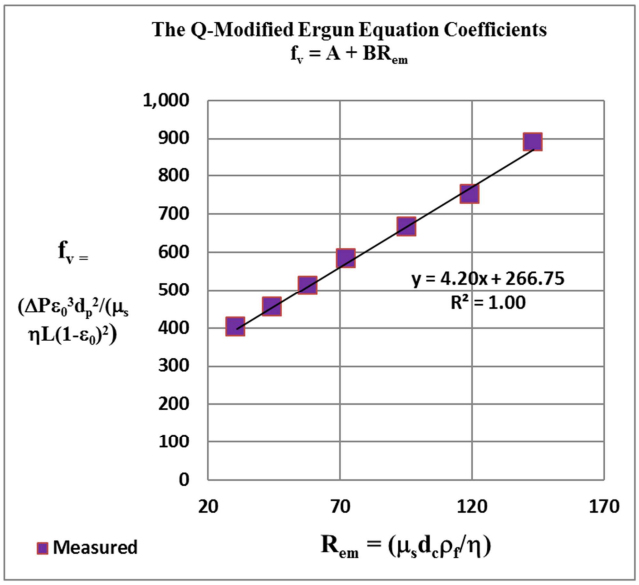

Figure 12. *The Q-modified Ergun equation.*

Step 7. Determine the Universal constants, k_1 and k_2.

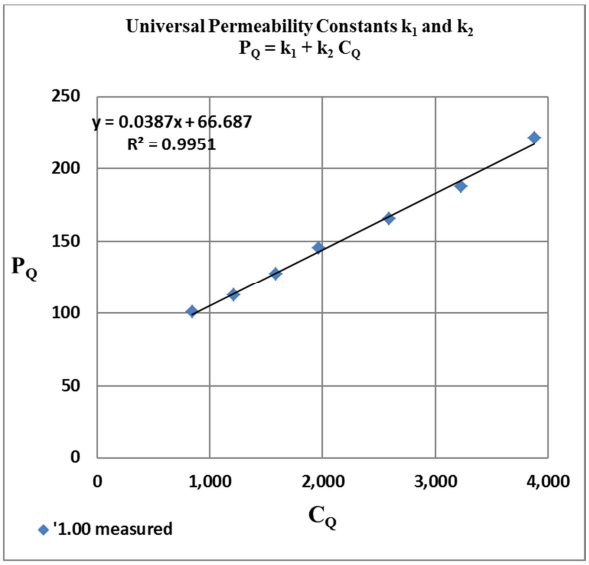

Figure 13. *Universal Quinn constants.*

Step 8. Compare the measured and calculated pressure drops.

As shown in Figure 14, the correlation between the measured and calculated values of ΔP is excellent. This step is critical to validate the methodology and *cannot be omitted* in any credible fluid flow model analysis.

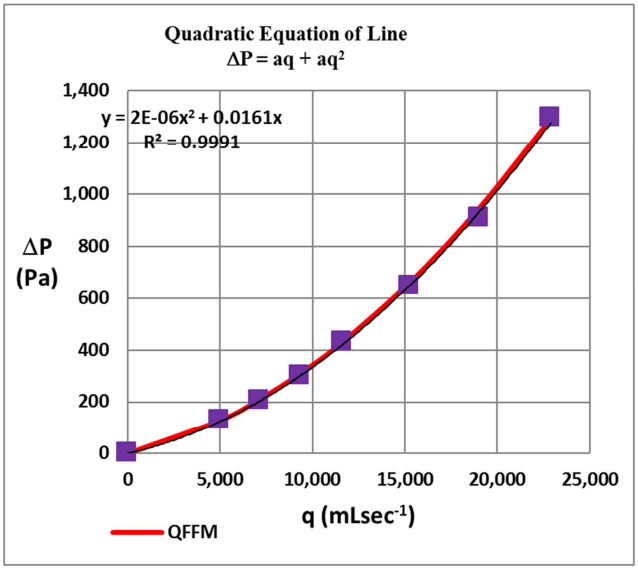

Figure 14. *Measured data versus calculated data.*

Step 9. Document a first data summary table.

Table 3. *First data summary.*

Sample ID	ΔP	Forchheimer		Q-Mod. Ergun			Net Wall Effect		Impact of λ		Univ. Consts.		
	$\Delta P = aq + bq^2$	$\Delta H = a\mu_s + b\mu_s^2$		$f_v = A + BR_{em}$			$W_N = W_1 + W_{2R}$		$\lambda = 1 + W_N$		$P_Q = k_1 + k_2 C_Q$		
		a	b	A	B	R^2	W_1	W_{2R}	k	λ	k_1	k_2	R^2
	Pa	$seccm^{-1}$	sec^2cm^{-2}	none	none	none	none	none	cm	none	none	none	none
1.00	$0.0161q + 2 x10\text{-}6 q^2$	2.5511	0.0754	268.19	4.17	0.9950	2 x 10-8	5.00	0.00120	5.99	67.05	0.0398	1.000
1.25	$0.0073q + 6 x10\text{-}7 q^2$	2.2397	0.0368	268.19	2.12	0.9790	2 x 10-8	2.30	0.00012	3.31	67.05	0.0398	1.000
1.60	$0.0219q + 1 x10\text{-}6 q^2$	1.3990	0.0414	268.19	3.34	0.9900	5 x 10-8	3.41	0.00052	4.40	67.05	0.0398	1.000
2.00	$0.0183q + 1 x10\text{-}6 q^2$	0.9114	0.0335	268.19	3.17	0.9900	1 x 10-7	2.72	0.00034	3.72	67.05	0.0398	1.000
2.50	$0.0207q + 2 x10\text{-}6 q^2$	0.5170	0.0294	268.19	3.67	0.9900	3 x 10-7	3.38	0.00089	4.39	67.05	0.0398	1.000
3.15	$0.0161q + 1 x10\text{-}6 q^2$	0.4894	0.0188	268.19	2.36	0.9940	3 x 10-7	1.74	0.00013	2.74	67.05	0.0398	1.000
4.00	$0.003q + 4 x10\text{-}7 q^2$	0.2883	0.0161	268.19	2.62	0.9990	7 x 10-7	2.18	0.00033	3.20	67.05	0.0398	1.000
5.00	$0.0052q + 6 x10\text{-}7 q^2$	0.2263	0.0128	268.19	2.33	0.9970	9 x 10-7	1.89	0.00023	2.88	67.05	0.0398	1.000
6.30	$0.0047q + 7 x10\text{-}7q^2$	0.1459	0.0110	268.19	2.50	0.9980	2 x 10-6	2.07	0.00038	3.07	67.05	0.0398	1.000
8.00	$0.0042q + 7 x10\text{-}7 q^2$	0.0893	0.0080	268.19	2.31	0.9960	4 x 10-6	1.74	0.00029	2.74	67.05	0.0398	1.000

Step 10. Document a second data summary table.

Table 4. *Second summary data.*

Sample ID	D	L	Conduit	Conduit	Hypoth.	Ext.	SPH. Part.	No.	Nom.	Part.	Part.
	Diam.	length	Archt.	Tortuosity	Channel	Porosity	Diam.	Parts.	Part.	Spher.	Porosity
			Coeff.		Diam.		Equiv.		Diam.		
			γ	τ	d_c	ε_0	d_p	n_p	d_{pm}	Ω_p	ε_p
	cm	cm	none	none	cm	none	cm	none	cm	none	none
1.00	19.4	15.7	1.E+07	4.E+07	0.261	0.606	0.103	3.19E+06	0.113	0.916	0
1.25	19.4	9.7	9.E+06	4.E+07	0.274	0.614	0.106	1.79E+06	0.143	0.742	0
1.60	19.4	27.1	4.E+06	2.E+07	0.354	0.604	0.140	2.20E+06	0.180	0.778	0
2.00	19.4	30.0	2.E+06	8.E+06	0.465	0.581	0.195	9.63E+05	0.225	0.865	0
2.50	19.4	49.5	6.E+05	3.E+06	0.614	0.583	0.256	6.97E+05	0.283	0.905	0
3.15	19.4	49.6	5.E+05	3.E+06	0.641	0.577	0.271	5.94E+05	0.358	0.759	0
4.00	19.4	19.1	2.E+05	1.E+06	0.823	0.583	0.343	1.11E+05	0.450	0.762	0
5.00	19.4	36.1	2.E+05	1.E+06	0.929	0.583	0.388	1.46E+05	0.565	0.686	0
6.30	19.4	44.2	1.E+05	5.E+05	1.158	0.583	0.483	9.24E+04	0.715	0.676	0
8.00	19.4	49.3	4.E+04	2.E+05	1.500	0.578	0.634	4.62E+04	0.703	0.704	0

Table 4 displays some of the more important values in this study. For instance, it demonstrates that the sphericity of the particles, Ω_p, varied from sample to sample, but was generally between the values of 0.7 and 0.9. We used as our

nominal particle diameter, d_{pm}, the average of the upper and lower vibratory screen openings, as a basis for estimating the sphericity. It also demonstrates the enormous value of the fluid path tortuosity, τ, in direct contradiction to what other fluid flow models teach.

Worked Example 2-Special case

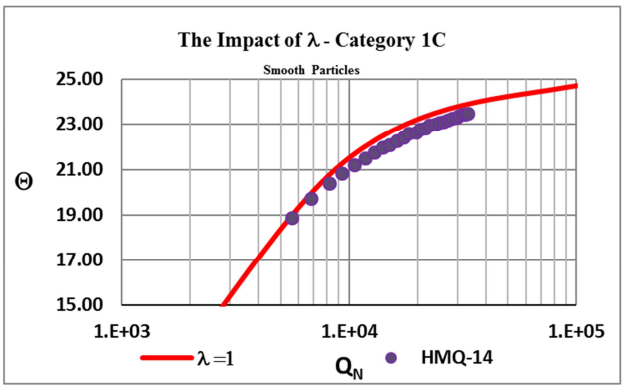

Figure 15. *Measureable wall effect.*

This is a special category of conduit packed with large glass beads in which the ratio of $D/d_p = 1.12$. We created this packed conduit so that we could count the number of glass beads, i.e., 297 which reconciles our value for the external porosity ε_0 [13]. This packed conduit has a measurable wall effect as is evidenced in the plot shown in Figure 15.

We want to emphasize that our methodology when applied to this special case or any empty conduit under study, must be modified to accommodate this special milieu of fluidic characteristics. The Forchheimer coefficients equivalent in this special case will not be constant. This is because of the ever-changing boundary layer, which means that the value of λ is different for each measured flow rate. Accordingly, in step 5 of our methodology outlined above the back-calculation must be done separately for each measured pressure drop and flow rate combination, in order to ensure that the correct value of λ is identified for each flow rate. We include here Table 5 to demonstrate the ever-changing value of the Forchheimer coefficient b equivalent, established as part of the back-calculation process.

Table 5. *The changing value of b.*

I.D.	q	a	b	λ	d_c	ε_0	d_p	n_p	k	$\Delta P_{(calc)}$	$\Delta P_{(meas)}$
	ml/sec	s/cm	s^2/cm^2		cm		cm		cm	Pa	Pa
HMQ - 14	0.92	0.0704	0.026082	1.030	0.618	0.467	0.329	297	0.00	24,355	24,355
1.	1.15	0.0704	0.026039	1.028	0.618	0.467	0.329	297	0.00	36,427	36,427
2.	1.38	0.0704	0.026004	1.027	0.618	0.467	0.329	297	0.00	50,872	50,872
3.	1.60	0.0704	0.025976	1.026	0.618	0.467	0.329	297	0.00	66,407	66,407
4.	1.82	0.0704	0.025953	1.025	0.618	0.467	0.329	297	0.00	83,985	83,985
5.	2.08	0.0704	0.025928	1.024	0.618	0.467	0.329	297	0.00	108,421	108,421
6.	2.27	0.0704	0.025913	1.023	0.618	0.467	0.329	297	0.00	127,013	127,013
7.	2.50	0.0704	0.025896	1.023	0.618	0.467	0.329	297	0.00	152,786	152,786
8.	2.72	0.0704	0.025882	1.022	0.618	0.467	0.329	297	0.00	178,835	178,835
9.	2.92	0.0704	0.025870	1.022	0.618	0.467	0.329	297	0.00	204,688	204,688
10.	3.13	0.0704	0.025858	1.021	0.618	0.467	0.329	297	0.00	234,653	234,653
11.	3.68	0.0704	0.025832	1.020	0.618	0.467	0.329	297	0.00	318,487	318,487
12.	3.53	0.0704	0.025839	1.020	0.618	0.467	0.329	297	0.00	295,322	295,322
13.	3.75	0.0704	0.025829	1.020	0.618	0.467	0.329	297	0.00	331,080	331,080
14.	3.97	0.0704	0.025820	1.020	0.618	0.467	0.329	297	0.00	368,873	368,873
15.	4.17	0.0704	0.025813	1.019	0.618	0.467	0.329	297	0.00	405,563	405,563
16.	4.42	0.0704	0.025804	1.019	0.618	0.467	0.329	297	0.00	453,863	453,863
17.	4.67	0.0704	0.025795	1.019	0.618	0.467	0.329	297	0.00	504,869	504,869
18.	4.88	0.0704	0.025789	1.018	0.618	0.467	0.329	297	0.00	551,264	551,264
19.	5.05	0.0704	0.025784	1.018	0.618	0.467	0.329	297	0.00	588,335	588,335
20.	5.25	0.0704	0.025778	1.018	0.618	0.467	0.329	297	0.00	634,407	634,407
21.	5.42	0.0704	0.025773	1.018	0.618	0.467	0.329	297	0.00	674,123	674,123
22.	5.67	0.0704	0.025767	1.018	0.618	0.467	0.329	297	0.00	735,951	735,951
23.	5.83	0.0704	0.025763	1.017	0.618	0.467	0.329	297	0.00	778,672	778,672
24.	6.17	0.0704	0.025755	1.017	0.618	0.467	0.329	297	0.00	867,720	867,720
25.	6.25	0.0704	0.025753	1.017	0.618	0.467	0.329	297	0.00	890,733	890,733
26.	6.42	0.0704	0.025749	1.017	0.618	0.467	0.329	297	0.00	937,660	937,660

As shown in Table 5, we have used our procedure outlined in step 5 above to back-calculate for the value of the b coefficient, by correlating the measured data for each measured flow rate. This is possible, in this particular case, because we have independently identified the number of particles present in the packed conduit, i.e., 297. We accomplished this by actually counting the number of perfectly spherical smooth glass beads present in the packed conduit. Note in the table that the value of b is slightly different for each measured data point.

Worked Example 3-Van Lopik et al

We chose this example because it is a very comprehensive study of varying the particle size distribution in packed conduits [14, 15]. Thus, this data base show off the ability of the QFFM to differentiate between conduits packed with different particle shapes and distributions.

The results of this worked example demonstrate that the QFFM can identify the impact of particle shape and distributions

via the calculated value of Ω_p, the particle sphericity, which is the "fudge factor" which normalizes for these variables.

Table 6. *Van Lopik first data summary.*

I.D.	Forchheimer		Q-Mod. Ergun		Net Wall Effect		Impact of λ		Univ. Consts.	
	$\Delta H = a\mu_s + b\mu_s^2$		$f_v = A + BR_{em}$		$W_N = W_1 + W_{2R}$		$\lambda = 1 + W_N$		$P_Q = k_1 + k_2C_Q$	
	a	b	A	B	W_1	W_{2R}	k	λ	k_1	k_2
	$sec cm^{-1}$	$sec^2 cm^{-2}$	none	none	none	none	cm	none	none	none
2017 d_{50} Reference										
1	19.2130	1.3541	268.19	3.42	0.00	0.00	0.00	1.00	67.05	0.0398
2	14.2650	1.2523	268.19	3.58	0.00	0.00	0.00	1.00	67.05	0.0398
3	6.9695	0.7008	268.19	3.09	0.00	0.00	0.00	1.00	67.05	0.0398
4	5.6216	0.6782	268.19	3.25	0.00	0.00	0.00	1.00	67.05	0.0398
5	3.5856	0.5641	268.19	3.34	0.00	0.00	0.00	1.00	67.05	0.0398
6	2.4575	0.4396	268.19	3.20	0.00	0.00	0.00	1.00	67.05	0.0398
7	2.4723	0.3881	268.19	2.94	0.00	0.00	0.00	1.00	67.05	0.0398
8	1.4060	0.3104	268.19	3.06	0.00	0.00	0.00	1.00	67.05	0.0398
9	1.0584	0.2489	268.19	2.90	0.00	0.00	0.00	1.00	67.05	0.0398
10	0.6450	0.1745	268.19	2.70	0.00	0.00	0.00	1.00	67.05	0.0398
11	0.0796	0.0611	268.19	2.70	0.00	0.00	0.00	1.00	67.05	0.0398
2017 d_{50} Composites										
3.1	7.4018	0.8220	268.19	3.37	0.00	0.00	0.00	1.00	67.05	0.0398
4.1	6.2357	0.7839	268.19	3.46	0.00	0.00	0.00	1.00	67.05	0.0398
5.1	4.1833	0.6349	268.19	3.43	0.00	0.00	0.00	1.00	67.05	0.0398
6.1	3.6231	0.5561	268.19	3.29	0.00	0.00	0.00	1.00	67.05	0.0398
6.2	3.2626	0.5182	268.19	3.25	0.00	0.00	0.00	1.00	67.05	0.0398
6.3	2.5680	0.4380	268.19	3.15	0.00	0.00	0.00	1.00	67.05	0.0398
6.4	4.1274	0.6351	268.19	3.45	0.00	0.00	0.00	1.00	67.05	0.0398
7.1	2.8351	0.4966	268.19	3.31	0.00	0.00	0.00	1.00	67.05	0.0398
8.1	1.6836	0.3519	268.19	3.13	0.00	0.00	0.00	1.00	67.05	0.0398
2019 d_{50} Blended										
M.1	15.9710	1.6572	268.19	4.16	0.00	0.00	0.00	1.00	67.05	0.0398
M.2	16.1250	1.4464	268.19	3.79	0.00	0.00	0.00	1.00	67.05	0.0398
M.3	13.3490	2.1103	268.19	5.19	0.00	0.00	0.00	1.00	67.05	0.0398
W.1	13.2610	3.6662	268.19	7.51	0.00	0.00	0.00	1.00	67.05	0.0398
W.2	2.6337	0.9958	268.19	5.40	0.00	0.00	0.00	1.00	67.05	0.0398
S.1	2.4723	0.3881	268.19	2.94	0.00	0.00	0.00	1.00	67.05	0.0398
1.1	4.0647	0.5723	268.19	3.23	0.00	0.00	0.00	1.00	67.05	0.0398
1.2	5.0505	0.7155	268.19	3.49	0.00	0.00	0.00	1.00	67.05	0.0398
1.3	7.2465	0.9701	268.19	3.79	0.00	0.00	0.00	1.00	67.05	0.0398
1.4	8.1194	1.4249	268.19	4.71	0.00	0.00	0.00	1.00	67.05	0.0398
1.5	14.1180	2.4222	268.19	5.58	0.00	0.00	0.00	1.00	67.05	0.0398
S.2	1.0498	0.2498	268.19	2.92	0.00	0.00	0.00	1.00	67.05	0.0398
2.1	1.5956	0.3282	268.19	3.05	0.00	0.00	0.00	1.00	67.05	0.0398
2.2	3.0529	0.5726	268.19	3.56	0.00	0.00	0.00	1.00	67.05	0.0398
2.3	5.8496	1.1219	268.19	4.48	0.00	0.00	0.00	1.00	67.05	0.0398
2.4	8.2669	1.6280	268.19	5.12	0.00	0.00	0.00	1.00	67.05	0.0398
2.5	15.7350	3.1612	268.19	6.43	0.00	0.00	0.00	1.00	67.05	0.0398
S.3	0.0796	0.0611	268.19	2.70	0.00	0.00	0.00	1.00	67.05	0.0398
3.1	0.4016	0.1577	268.19	2.96	0.00	0.00	0.00	1.00	67.05	0.0398
3.2	1.6384	0.6187	268.19	4.61	0.00	0.00	0.00	1.00	67.05	0.0398
3.3	2.8755	0.8941	268.19	4.88	0.00	0.00	0.00	1.00	67.05	0.0398

Table 7. *Van Lopik second data summary.*

Sample ID	D	L	Conduit	Conduit	Hypoth.	Ext.	SPH. Part.	No.	Nom.	Part.	Part.
	Diam.	length	Archt. Coeff.	Tortuosity	Channel Diam.	Porosity	Diam. Equiv.	Parts.	Part. Diam.	Spher.	Porosity
			γ	τ	d_c	ε_0	d_p	n_p	d_{pm}	Ω_p	ε_p
	cm	cm	none	none	cm	none	cm	none	cm	none	none
2017 d_{50} Reference											
1	9.8	50.7	3.E+07	7.E+08	0.055	0.360	0.035	1.05E+08	0.039	0.908	0
2	9.8	50.7	2.E+07	4.E+08	0.066	0.354	0.042	6.17E+07	0.039	1.088	0

Sample ID	D	L	Conduit	Conduit	Hypoth.	Ext.	SPH. Part.	No.	Nom.	Part.	Part.
	Diam.	length	Archt. Coeff.	Tortuosity	Channel Diam.	Porosity	Diam. Equiv.	Parts.	Part. Diam.	Spher.	Porosity
			γ	τ	d_c	ε_0	d_p	n_p	d_{pm}	Ω_p	ε_p
	cm	cm	none	none	cm	none	cm	none	cm	none	none
3	9.8	50.7	9.E+06	2.E+08	0.087	0.372	0.055	2.79E+07	0.061	0.899	0
4	9.8	50.7	6.E+06	1.E+08	0.100	0.366	0.063	1.84E+07	0.071	0.890	0
5	9.8	50.7	3.E+06	6.E+07	0.126	0.363	0.081	8.89E+06	0.084	0.960	0
6	9.8	50.7	2.E+06	3.E+07	0.150	0.368	0.095	5.44E+06	0.099	0.956	0
7	9.8	50.7	2.E+06	4.E+07	0.143	0.378	0.089	6.45E+06	0.105	0.847	0
8	9.8	50.7	8.E+05	2.E+07	0.193	0.373	0.121	2.57E+06	0.136	0.891	0
9	9.8	50.7	6.E+05	1.E+07	0.217	0.380	0.135	1.85E+06	0.150	0.898	0
10	9.8	50.7	3.E+05	5.E+06	0.268	0.389	0.164	1.01E+06	0.211	0.777	0
11	9.8	50.7	1.E+04	2.E+05	0.763	0.389	0.466	4.40E+04	0.634	0.735	0
2017 d_{50} Composites											0
3.1	9.8	50.7	8.E+06	2.E+08	0.088	0.361	0.056	2.59E+07	0.062	0.915	0
4.1	9.8	50.7	6.E+06	1.E+08	0.098	0.358	0.063	1.91E+07	0.071	0.878	0
5.1	9.8	50.7	3.E+06	7.E+07	0.119	0.359	0.076	1.06E+07	0.084	0.904	0
6.1	9.8	50.7	3.E+06	6.E+07	0.125	0.364	0.079	9.25E+06	0.099	0.800	0
6.2	9.8	50.7	2.E+06	5.E+07	0.131	0.366	0.083	8.09E+06	0.099	0.840	0
6.3	9.8	50.7	2.E+06	4.E+07	0.145	0.370	0.092	6.00E+06	0.099	0.925	0
6.4	9.8	50.7	3.E+06	7.E+07	0.120	0.359	0.077	1.03E+07	0.101	0.763	0
7.1	9.8	50.7	2.E+06	4.E+07	0.142	0.363	0.090	6.33E+06	0.105	0.861	0
8.1	9.8	50.7	1.E+06	2.E+07	0.179	0.370	0.113	3.22E+06	0.136	0.826	0
2019 d_{50} Blended											
M.1	9.8	50.7	2.E+07	4.E+08	0.067	0.337	0.044	5.55E+07	0.045	0.986	0
M.2	9.8	50.7	2.E+07	5.E+08	0.064	0.348	0.041	6.69E+07	0.054	0.767	0
M.3	9.8	50.7	8.E+06	3.E+08	0.082	0.313	0.056	2.84E+07	0.077	0.729	0
W.1	9.8	50.7	4.E+06	2.E+08	0.099	0.277	0.071	1.45E+07	0.148	0.482	0
W.2	9.8	50.7	6.E+05	2.E+07	0.188	0.309	0.130	2.31E+06	0.950	0.137	0
S.1	9.8	50.7	2.E+06	4.E+07	0.143	0.378	0.089	6.45E+06	0.105	0.847	0
1.1	9.8	50.7	3.E+06	7.E+07	0.117	0.367	0.074	1.14E+07	0.105	0.705	0
1.2	9.8	50.7	4.E+06	9.E+07	0.109	0.357	0.070	1.37E+07	0.105	0.667	0
1.3	9.8	50.7	6.E+06	1.E+08	0.095	0.348	0.062	2.02E+07	0.105	0.589	0
1.4	9.8	50.7	5.E+06	1.E+08	0.100	0.323	0.068	1.60E+07	0.105	0.644	0
1.5	9.8	50.7	8.E+06	3.E+08	0.082	0.305	0.057	2.70E+07	0.105	0.545	0
S.2	9.8	50.7	6.E+05	1.E+07	0.219	0.379	0.136	1.81E+06	0.150	0.905	0
2.1	9.8	50.7	1.E+06	2.E+07	0.181	0.374	0.113	3.14E+06	0.150	0.756	0
2.2	9.8	50.7	2.E+06	4.E+07	0.141	0.355	0.091	6.20E+06	0.150	0.608	0
2.3	9.8	50.7	3.E+06	9.E+07	0.115	0.329	0.077	1.07E+07	0.150	0.514	0
2.4	9.8	50.7	4.E+06	1.E+08	0.103	0.314	0.071	1.42E+07	0.150	0.472	0
2.5	9.8	50.7	7.E+06	3.E+08	0.084	0.291	0.059	2.47E+07	0.150	0.396	0
S.3	9.8	50.7	1.E+04	2.E+05	0.763	0.389	0.466	4.40E+04	0.634	0.735	0
3.1	9.8	50.7	1.E+05	2.E+06	0.356	0.377	0.222	4.18E+05	0.634	0.349	0
3.2	9.8	50.7	4.E+05	1.E+07	0.220	0.326	0.148	1.51E+06	0.634	0.234	0
3.3	9.8	50.7	9.E+05	3.E+07	0.171	0.319	0.116	3.16E+06	0.634	0.183	0

Worked Example 4-Neue et al

This is an example taken from the field of HPLC (High pressure Liquid Chromatography) [16]. The particles are very small, less than 2 micron in diameter, are spherical and porous, i.e., $\varepsilon_p = 0.578$.

Table 8. *Neue first data summary.*

Sample ID	ΔP	Forchheimer		Q-Mod. Ergun			Net Wall Effect		Impact of λ		Univ. Consts.		
	$\Delta P = aq + bq^2$	$\Delta H = a\mu_s + b\mu_s^2$		$f_v = A + BR_{em}$			$W_N = W_1 + W_{2R}$		$\lambda = 1 + W_N$		$P_Q = k_1 + k_2 C_Q$		
		a	b	A	B	R^2	W_1	W_{2R}	k	λ	k_1	k_2	R^2
	Pa	$seccm^{-1}$	sec^2cm^{-2}	none	none	none	none	none	cm	none	none	none	none
1	$5 \times 10^{10}q + 6 \times 10^8q^2$	374,308	141	268.19	2.50	1.00	0.00	0.00	0.00000	1.00	67.05	0.0398	1.00
2	$8 \times 10^9 q + 3 \times 10^8 q^2$	56,486	66	268.19	2.84	1.00	0.00	0.00	0.00000	1.00	67.05	0.0398	1.00
3	$3 \times 10^{10} q + 3 \times 10^8 q^2$	376,635	142	268.19	2.51	1.00	0.00	0.00	0.00000	1.00	67.05	0.0398	1.00
4	$2 \times 10^{10} q + 5 \times 10^8 q^2$	56,486	66	268.19	2.84	1.00	0.00	0.00	0.00000	1.00	67.05	0.0398	1.00

Table 9. *Neue second data summary.*

Sample ID	D	L	Conduit	Conduit	Hypoth.	Ext.	SPH. Part.	No.	Nom.	Part.	Part.
	Diam.	length	Archt. Coeff.	Tortuosity	Channel Diam.	Porosity	Diam. Equiv.	Parts.	Part. Diam.	Spher.	Porosity
			γ	τ	d_c	ε_0	d_p	n_p	d_{pm}	Ω_p	ε_p
	cm	cm	none	none	cm	none	cm	none	cm	none	none
1	0.21	5.0	3.E+09	4.E+10	2.83E-04	0.399	1.7E-04	4.03E+10	1.7E-04	1.00	0.578
2	0.21	5.0	1.E+08	2.E+09	7.78E-04	0.383	4.8E-04	1.85E+09	4.8E-04	1.00	0.578
3	0.21	3.0	3.E+09	4.E+10	2.83E-04	0.399	1.7E-04	2.43E+10	1.7E-04	1.00	0.578
4	0.21	10.0	1.E+08	2.E+09	7.78E-04	0.383	4.8E-04	3.69E+09	4.8E-04	1.00	0.578

Worked Example 5-Cabooter et al

This example is also taken from the field of HPLC [17]. The particles are porous in all 6 conduits. Note that in the samples numbered 5 and 6, the particles are identical to those used in the Neue example above. However, in these packed conduits, the particle porosity is significantly decreased which suggests that the particles are compressed due to the enormous packing pressures used (20,000 psi). Accordingly, this example demonstrates the ability of the QFFM to evaluate particle porosity which is an additional significant advantage over other fluid flow models.

Table 10. *Cabooter first data summary.*

Sample ID	ΔP	Forchheimer		Q-Mod. Ergun			Net Wall Effect		Impact of λ		Univ. Consts.		
	$\Delta P = aq + bq^2$	$\Delta H = a\mu_s + b\mu_s^2$		$f_v = A + BR_{em}$			$W_N = W_1 + W_{2R}$		$\lambda = 1 + W_N$		$P_Q = k_1 + k_2 C_Q$		
		a	b	A	B	R^2	W_1	W_{2R}	k	λ	k_1	k_2	R^2
	Barye	$seccm^{-1}$	sec^2cm^{-2}	none	none	none	none	none	cm	none	none	none	none
1	$3.51 \times 10^{10}q + 1.97 \times 10^{8}q^2$	349,159	68.02	268.19	2.03	1.00	0.00	0.00	0.00	1.00	67.05	0.0398	1.00
2	$4.00 \times 10^{10}q + 2.38 \times 10^{8}q^2$	398,449	82.34	268.19	1.87	1.00	0.00	0.00	0.00	1.00	67.05	0.0398	1.00
3	$4.67 \times 10^{10}q + 2.76 \times 10^{8}q^2$	464,173	95.16	268.19	2.13	1.00	0.00	0.00	0.00	1.00	67.05	0.0398	1.00
4	$9.50 \times 10^{9}q + 1.16 \times 10^{7}q^2$	453,322	92.01	268.19	2.10	1.00	0.00	0.00	0.00	1.00	67.05	0.0398	1.00
5	$4.62 \times 10^{10}q + 2.32 \times 10^{8}q^2$	460,066	79.97	268.19	1.09	1.00	0.00	0.00	0.00	1.00	67.05	0.0398	1.00
6	$4.95 \times 10^{10}q + 2.63 \times 10^{8}q^2$	492,927	90.80	268.19	2.02	1.00	0.00	0.00	0.00	1.00	67.05	0.0398	1.00

Table 11. *Cabooter second data summary.*

I.D.	D	L	γ	τ	d_c	dp	ε_0	d_{pm}	Ω_p	n_p	ε_p
Cabooter 2008	cm	cm	none	none	cm	cm	none	cm	none	none	none
Hypersil Gold C18											
1 Hypersil Gold C18	0.21	5.00	2.21E+09	2.60E+10	3.29E-04	1.845E-04	0.4398	1.900E-04	0.971	2.95E+10	0.345
2 Zorbax C18	0.21	5.00	2.23E+09	2.85E+10	3.21E-04	1.839E-04	0.4278	1.900E-04	0.968	3.04E+10	0.302
3 Zorbax C18	0.21	5.00	2.53E+09	3.39E+10	3.05E-04	1.763E-04	0.4213	1.800E-04	0.980	3.49E+10	0.240
4 Acquity BEH C18	0.46	5.00	2.66E+10	3.50E+11	3.06E-04	1.765E-04	0.4234	1.800E-04	0.981	1.66E+11	0.200
5 Acquity BEH C18	0.21	5.00	3.23E+09	3.85E+10	2.89E-04	1.627E-04	0.4350	1.700E-04	0.957	4.32E+10	0.325
6	0.21	5.00	3.11E+09	3.95E+10	2.88E-04	1.647E-04	0.4286	1.700E-04	0.969	4.23E+10	0.281

5. Conclusions

In this paper we have used the QFFM to demonstrate that permeability measurements can be used as a starting point in a back-calculation process to identify the values of the input variables, of d_p, and ε_o in packed conduits. This is a significant advancement over all prior fluid flow models since it is effective even when the particle shape and roughness does not permit accurate measurements of particle size dimensions, on the one hand, and when the wall effect manifests, on the other hand. Moreover, by establishing the standardized methodology outlined herein, this paper defines the gold standard of how to systematically design, execute and report permeability studies on packed conduits containing porous media, which applies equally well to conduits packed with solid particles as well as empty conduits, i.e., conduits packed with fully porous particles.

Declaration and Statements

The author has no financial or nonfinancial interests in this publication.

References

[1] Quinn, H. M. Quinn's Law of Fluid Dynamics Pressure-driven Fluid Flow Through Closed Conduits, *Fluid Mechanics*. Vol. 5, No. 2, 2019, pp. 39-71. doi: 10.11648/j.fm.20190502.12.

[2] Ergun, S. and Orning, A. A., Fluid Flow through Randomly Packed Columns and Fluidized Beds, Ind. Eng. Chem. vol. 41, pp. 1179, 1949.

[3] Farkas, T., G. Zhong, G. Guiochon, Validity of Darcy's Law at Low Flow Rates in Liquid Chromatography Journal of Chromatography A, 849, (1999) 35-43.

[4] Quinn, H. M., A Reconciliation of Packed Column Permeability Data: Deconvoluting the Ergun Papers Journal of Materials Volume 2014 (2014), Article ID 548482, 24 pages http://dx.doi.org/10.1155/2014/548482.

[5] Quinn, H. M., Quinn's Law of Fluid Dynamics: Supplement #1 Nikuradze's Inflection Profile Revisited. *Fluid Mechanics*. Vol. 6, No. 1, 2020, pp. 1-14. doi: 10.11648/j.fm.20200601.11.

[6] Quinn, H. M., Quinn's Law of Fluid Dynamics: Supplement #2 Reinventing the Ergun Equation. *Fluid Mechanics*. Vol. 6, No. 1, 2020, pp. 15-29. doi: 10.11648/j.fm.20200601.12.

[7] Nikuradze J., NASA TT F-10, 359, Laws of Turbulent Flow in Smooth Pipes. Translated from "Gesetzmassigkeiten der turbulenten Stromung in glatten Rohren" VDI (Verein Deutsher Ingenieure)-Forschungsheft 356.

[8] Mckeon, B. J. C. J. Swanson, M. V. Zagarola, R. J. Donnelly and A. J. Smits. Friction factors for smooth pipe flow; J. Fluid Mech. (2004), vol. 511, pp. 41-44. Cambridge University Press; DO1; 10.1017/S0022112004009796.

[9] Mckeon, B. J., M. V. Zagarola, and A. J. Smits. A new friction factor relationship for fully developed pipe flow; J. Fluid Mech. (2005), vol. 238, pp. 429-443. Cambridge University Press; DO1; 10.1017/S0022112005005501.

[10] Buchwald T., Gregor Schmandra, Lieven Schützenmeister, Tony Fraszczak, Thomas Mütze, Urs Peuker Gaseous flow through coarse granular beds: The role of specific surface area; Powder Technology 366 (2020) 821-831.

[11] Nikuradze J., NACA TM 1292, Laws of Flow in Rough Pipes, July/August 1933. Translation of "Stromungsgesetze in rauhen Rohren." VDI-Forschungsheft 361. Beilage zu "Forschung auf dem Gebiete des Ingenieurwesens" Ausgabe B Band 4, July/August 1933.

[12] Forchheimer, P.: Wasserbewegung durch boden. Zeit. Ver. Deutsch. Ing 45, 1781–1788 (1901).

[13] Quinn Hubert Michael. Quinn's Law of Fluid Dynamics: Supplement #3 A Unique Solution to the Navier-Stokes Equation for Fluid Flow in Closed Conduits. Fluid Mechanics. Volume 6, Issue 2, December 2020, pp. 30-50. doi: 10.11648/j.fm.20200602.11.

[14] Van Lopik Jan H. Roy Snoeijers Teun C. G. W. van Dooren Amir Raoof Ruud J. Schotting; Transp Porous Med (2017) 120: 37–66 DOI 10.1007/s11242-017-0903-3.

[15] Van Lopik Jan H. Roy, L. Zazai · N. Hartog, R. J. Schotting, Nonlinear Flow Behavior in Packed Beds of Natural and Variably Graded Granular Materials Transport in Porous Media (2019) 131: 957–983 https://doi.org/10.1007/s11242-019-01373-0

[16] U. D. Neue J. Mazzeo, M. Kele, R. S. Plumb; Analytical Chemistry, December 2005, 460-467.

[17] Cabooter D., J. Billen, H. Terryn, F. Lynen, P. Sandra, G. Desmet; Journal of Chromatography A, 1178 (2008) 108–117.